energies

MDPI

Article

Research on Sub-Synchronous-Oscillation Energy Analysis and Traceability Method Based on Refined Energy

Zhixiang Zhang [1], Jingying Yang [2], Shuyu Zhou [1,3], Cheng Liu [1,*], Song Gao [3] and Zhichong Cao [1]

[1] School of Electrical Engineering, Northeast Electric Power University, Jilin 132012, China; b861720023@163.com (Z.Z.); zzhousy@163.com (S.Z.); caozhichongq@163.com (Z.C.)
[2] State Grid Jilin Electric Power Company Limited, Changchun 130028, China; aazyc11600@163.com
[3] State Grid Jilin Electric Power Research Institute, Changchun 130021, China; gaosong84698822@126.com
* Correspondence: liucheng@neepu.edu.cn

Abstract: At present, most studies use the direct method to analyze the oscillation problem of modern power systems. However, these studies often only simplify the external characteristics of the wind turbine and lack an in-depth understanding of its internal refined energy structure. In this paper, based on the direct-drive permanent magnetic synchronous generator's detailed model (D-PMSG), combined with the dynamic energy of its port, layers of analysis are performed on the wind turbine's internal connections, and a detailed model of the energy structure is created. Then, the interaction mechanism of each control link in the wind turbine is analyzed by combining the energy function of the wind turbine with the improved perturbation method. Finally, this paper constructs a sub-synchronous oscillation (SSO) scenario of weak damping and a forcing type and proves the accuracy and effectiveness of the traceability method based on the refined energy of D-PMSG. This traceability method based on refined energy is expected to provide a new solution to the stability problem caused by the integration of new energy.

Keywords: sub-synchronous oscillation; refined modeling; energy function; direct-drive permanent magnetic synchronous generator

check for updates

Citation: Zhang, Z.; Yang, J.; Zhou, S.; Liu, C.; Gao, S.; Cao, Z. Research on Sub-Synchronous-Oscillation Energy Analysis and Traceability Method Based on Refined Energy. *Energies* **2024**, *17*, 1683. https://doi.org/10.3390/en17071683

Academic Editor: Daniel Morinigo-Sotelo

Received: 24 January 2024
Revised: 23 March 2024
Accepted: 28 March 2024
Published: 1 April 2024

Copyright: © 2024 by the authors. Licensee MDPI, Basel, Switzerland. This article is an open access article distributed under the terms and conditions of the Creative Commons Attribution (CC BY) license (https://creativecommons.org/licenses/by/4.0/).

1. Introduction

The large-capacity, long-distance cross-regional transmission characteristics of new energy present significant obstacles to power systems' ability to dampen and regulate, making power-system stability issues even more complicated and challenging to handle in the face of minor disturbances. Following widespread use of power electronic equipment, the system's inertia decreases, immunity is compromised, and the power oscillation's amplitude greatly increases [1,2]. Among them, the problem of SSO caused by the access of D-PMSG to weak AC systems is becoming more and more prominent. Since 2009, SSO problems have occurred in wind farms in Texas and Guyuan [3], North China. These accidents lead to several wind turbines being off the grid, which has a significant effect on the wind farm's regular operations. In these two accidents, experts have investigated the SSO issue in great detail [4,5] of doubly fed wind turbines and discussed causes and solutions. However, it is worth noting that a direct-drive wind farm in Hami, Xinjiang, China, also experienced continuous power SSO problems. Unlike the previous doubly fed wind turbine [6], this time involves D-PMSGs. The occurrence of this accident has attracted much attention from experts and scholars because D-PMSGs occupy an increasingly important position in wind farms [7]. The accident not only caused the loss of the wind farm itself but also led to the tripping of the adjacent thermal power units, which had an effect on the stability of the entire power system. This accident has aroused the attention and research of experts and scholars on the SSO problem of D-PMSGs.

With the continuous expansion of wind farms and the increase in new energy penetration, the effect of sub-synchronous oscillation on power-system stability is becoming more and

more prominent. Therefore, the in-depth study of the SSO problem of D-PMSGs not only helps to improve the operational stability of wind farms but also helps to promote the further development of new energy technologies. In wind farms, The SSO phenomenon is explained by the negative damping theory. SSO may occur when the sub-synchronous mode has negative damping characteristics. Although the oscillation problem is frequently studied using the direct technique, the understanding of the internal energy structure of the wind turbine is not deep enough. Some scholars believe that the SSO problem about wind farms is associated with forced-disturbance sources [8]. Through the forced-SSO theory, the generation mechanism of the three features is understood. These characteristics are generated by the system's feeble damping-SSO mode excited by the forced-disturbance source.

In addition, the authors of ref. [9] pointed out that one potential source of disturbance for forced SSO is the sub-synchronous interharmonics produced by the wind turbine converter. With the aim of controlling SSO, it is very important to identify its source quickly and accurately, including negative-damping and forcing types. Therefore, the traceability analysis of SSO is of practical significance, which is helpful to better understand the SSO problem of wind farms and take appropriate control measures. The authors of Reference [10] constructed an SSO-traceability architecture based on sub/super-synchronous phasor wide-area monitoring. It is possible to pinpoint the exact cause of the SSO by computing the sub-synchronous power flow of the entire system and using the power criterion. A real-time approach based on measurement data was presented in reference [11] to determine which wind farms are the biggest contributors to SSO. This technique tracks the amount and direction of sub-synchronous power produced by various wind farms or wind turbines in order to quantify and identify important wind farms. Many researchers believe that the energy-based oscillation-tracing method [12–14] has a wide range of practical application prospects [13]. This method can more accurately reflect the interaction mechanism of energy inside the system and offers a fresh perspective on resolving the power system stability issue brought on by the new energy-grid link. The transient energy-flow approach has shown impressive results in the localization of power-oscillation sources [15]. In the practical system application of ISO New England, this method is successfully applied to the online oscillation-management system, which automatically processes a large number of actual oscillation events and accurately identifies the low-frequency oscillation sources.

When dealing with SSO-disturbance-source location [16,17], the existing methods usually can only attribute the problem to a specific wind turbine, but lacks in-depth research on the internal control links of the wind turbine. This constraint could result in a lack of understanding of the oscillation's underlying cause, thus affecting effective control and management [18]. Based on the fine model of the D-PMSG converter, this paper not only analyzes the internal links of D-PMSG in detail but also accurately models its energy structure. This analysis method aims to understand the working principle and dynamic characteristics of D-PMSG more deeply [19,20]. By constructing an energy function that is capable of capturing D-PMSG's dynamic properties and fully taking into account the impact of its internal control connection, the disturbance source of the specific control link can be located more accurately. This research provides a more solid and comprehensive theoretical basis for the modeling and coordinated control of high-proportion renewable energy systems. The establishment of this theoretical basis not only helps to enhance the grid-connected stability of renewable energy but also helps to promote the optimization and upgrading of the entire energy system. It offers a fresh viewpoint and methodology for future research and facilitates the continued advancement and use of innovative energy technology [21].

2. Construction and Analysis of Fine Energy Function of D-PMSG Grid-Connected System

In this section, the construction of each control link's tiny signal model comes after the topological makeup of the D-PMSG linked to a weak AC power grid has been established. Combined with the transient energy-function equation, the refined energy function of D-PMSG including each control link is derived.

2.1. System Topology Structure

Figure 1 shows the topological structure of the system used in this paper. It includes two parts: a D-PMSG subsystem composed of 50 2 MW D-PMSGs and a weak AC system with a short circuit ratio (SCR) of 2.4. SCR is an indicator used to measure the relative strength of the D-PMSG and photovoltaic equipment input to the AC system. In general, when the SCR of the wind turbine is high (for example, greater than or equal to 3), the risk of an oscillation divergence of the wind turbine is low. On the contrary, when the SCR of the wind turbine access point is low (for example, less than 2, or even close to 1), the risk of an unstable oscillation of the wind turbine will increase. The parameters used in the emulation process are shown in Table 1, containing some reference values of the system and PI parameters of the converter control.

$$SCR = \frac{S_B}{S_W} = \frac{U_N^2}{Z_B S_W} \tag{1}$$

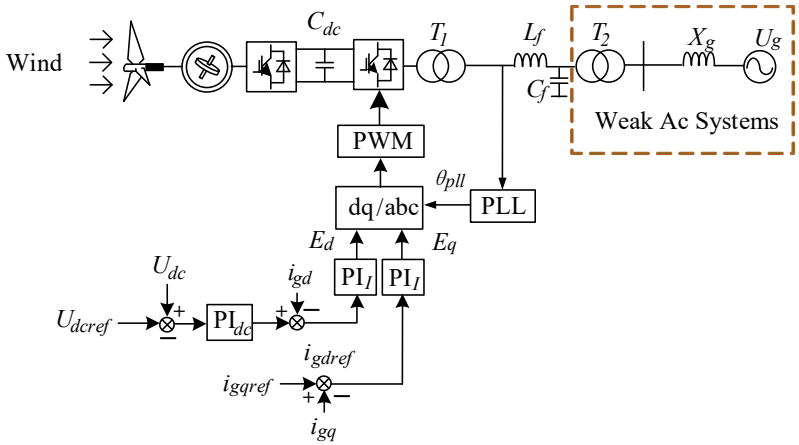


Figure 1. Grid-connected topology structure of D-PMSGs.

Table 1. Parameters used in the simulation process.

	Parameters	Numerical Value
System reference value	Line-voltage reference value V_{base}	690 V
	Frequency reference value f_{base}	50 Hz
	Power reference value S_{base}	2 MW
	Normal grid inductance L_g	0.63 mH
	Weak grid inductance L_{g1}	1.7 mH
Parameters of D-PMSG	DC capacitor C_{dc}	0.1 F
	Filter inductance L_f	0.1 p.u.
	Grid-side d-axis current control parameters k_{pd}, k_{id}	0.3, 160
	DC voltage control reference value U_{dcref}	1 p.u.
	DC voltage control parameters k_{pdc}, k_{idc}	3.5, 140
	Phase-locked control parameters k_{pp}, k_{ip}	50, 2000
	Grid-side q-axis current-control parameters k_{pq}, k_{iq}	0.3, 160

In the equation, U_N is the rated voltage of the system; Z_B is the equivalent impedance from the grid-connected point to the AC system; and S_W is the total capacity of the wind turbine. S_B is the short-circuit capacity of the AC system at the grid-connected point.

2.2. Small Signal Model of Each Control Link

The SSO phenomena resulting from D-PMSG access to the system frequently originate from the interaction between the grid-side converter and the weak AC grid. As a result, the

operation of these grid-side converter control linkages and the interaction of the control loops will be the main topics of this paper.

(1) Small signal model of the current loop

The current loop adopts classical PI control, and its control equation is the following:

$$\begin{cases} u_d = (k_{pd} + k_{id}\frac{1}{s})(i_{dref} - i_d) - \omega L_f i_q + e_{gd} \\ u_q = (k_{pq} + k_{iq}\frac{1}{s})(i_{qref} - i_q) + \omega L_f i_d + e_{gq} \end{cases} \tag{2}$$

In the equation, the q-axis-current loop's PI parameters are k_{pq} and k_{iq}, while u_d and u_q are the dq-axis voltage of the current-loop control output, respectively. The d-axis-current reference value is denoted by i_{dref}, while the q-axis current reference value is designated as a constant value during model construction. The filter inductance is denoted by l_f, and the dq axis grid voltage feedforward terms are e_{gd} and e_{gq}. The system angular frequency is represented by w, and the PI parameters of the d-axis current loop are k_{pd} and k_{id}. Separately, the dq axis currents are represented separately by i_d and i_q.

Linearization analysis of the above equation yields the following equation:

$$\begin{cases} \Delta u_d = (k_{pd} + k_{id}\frac{1}{s})(\Delta i_{dref} - \Delta i_d) - \omega_0 L_f \Delta i_q - \Delta\omega L_f i_{q0} + \Delta e_{gd} \\ \Delta u_q = -(k_{pq} + k_{iq}\frac{1}{s})\Delta i_q + \Delta\omega L_f i_{d0} + \omega_0 L_f \Delta i_d + \Delta e_{gq} \end{cases} \tag{3}$$

In the equation, the system's steady-state values of angular frequency, w_0, and dq axis current, i_{d0} and i_{q0}, are represented in the equation.

(2) Small signal model of DC voltage loop

The equation related to DC voltage-control can be expressed as the following:

$$U_{dc} = \sqrt{2(P_{in} - P)/(sC_{dc})} \tag{4}$$

$$i_{dref} = (U_{dc} - U_{dcref})(k_{pdc} + k_{idc}/s) \tag{5}$$

In the equation: the voltage of the DC capacitor is U_{dc}. The DC capacitor voltage reference value is U_{dcref}. P_e is the network side's input power, whereas P_{in} is the machine side's output power; C indicates the DC capacitor; and k_{pdc} and k_{idc} are PI parameters of the DC voltage loop.

By linearizing Equations (4) and (5) at the working point, the following equations are obtained:

$$\Delta U_{dc} = \frac{1}{sC_{dc}U_{dc0}}(\Delta P_{in} - \Delta P_e) \tag{6}$$

$$\Delta i_{dref} = \Delta U_{dc}(k_{pdc} + k_{idc}/s) = \frac{(k_{pdc} + k_{idc}/s)}{sC_{dc}U_{dc0}}(\Delta P_{in} - \Delta P_e) \tag{7}$$

$$\Delta P_e = 1.5(u_{d0}\Delta i_d + \Delta u_d i_{d0} + u_{q0}\Delta i_q + \Delta u_q i_{q0}) \tag{8}$$

(3) The linearization model of PLL is as follows:

$$\Delta\theta_{pll} = \frac{k_{ip} + sk_{pp}}{s^2}\Delta u_q \tag{9}$$

$$d\Delta\theta_{pll} = \int k_{ip}\Delta u_q dt + k_{pp}\Delta u_q \tag{10}$$

In the equation, k_{pp}, k_{ip} are the loop's PI parameters; the phase-locked loop voltage at the grid-connected point of the D-PMSG is utilized as an input, yet the phase-locked loop output is expressed by θ_{pll}. The phase-locked error angle of the phase-locked loop output can be represented by $\Delta\theta_{pll}$.

2.3. Refined Energy Function Construction of D-PMSG

In the analysis of SSO, this paper focuses on whether D-PMSG emits energy or absorbs energy, and judges whether D-PMSG provides positive damping or negative damping for the system, so as to judge whether the disturbance source is inside the D-PMSG.

Using the port node information of D-PMSG, the transient energy can be obtained as follows:

$$\begin{aligned} \Delta V &= \int \mathrm{Im}(-\Delta i_G^* d\Delta u_G) \\ &= \int \Delta i_d d\Delta u_q - \Delta i_q d\Delta u_d + \int \Delta P_e d\Delta \theta_{pll} \end{aligned} \tag{11}$$

The aforementioned equation shows that the former energy is connected to the port's voltage and current on the dq axis; the latter denotes the dynamic energy component directly determined by the phase-locked loop and the active power.

This is expanded as follows:

$$\begin{aligned} \Delta V &= \int \Delta i_d d\Delta u_q - \Delta i_q d\Delta u_d + \int \Delta P_e d\Delta \theta_{pll} = \int \Delta i_d d\Delta u_q - \Delta i_q d\Delta u_d + \int \Delta P_e \Delta \omega_{pll} dt \\ &= \int \begin{array}{l} [\Delta i_d(-(k_{pq}s + k_{iq})\Delta i_q + s\Delta\omega L_f i_{d0} + s\omega_0 L_f \Delta i_d + s\Delta e_{gq}) \\ -\Delta i_q(sk_{pd} + k_{id})(\Delta i_{dref} - \Delta i_d) - s\omega_0 L_f \Delta i_q - s\Delta\omega L_f i_{q0} + s\Delta e_{gd})] \end{array} dt \\ &+ \int -C_{dc} U_{dc0} \Delta U_{dc}(k_{ip}\Delta u_q + k_{pp}\Delta u_q s) dt \end{aligned} \tag{12}$$

The energy of each control link of D-PMSG can be obtained by combining Equations (12) and (3):

The energy expression dominated by the DC voltage control link is as follows:

$$\Delta V_{dc} = \int -\Delta i_q \Delta U_{dc}(sk_{pd} + k_{id})(k_{pdc} + k_{idc}/s) dt \tag{13}$$

The energy expression dominated by the current loop is as follows:

$$\begin{aligned} \Delta V_I &= \int -\Delta i_d \Delta i_q (k_{pq}s + k_{iq}) dt \\ &+ \int \Delta i_d (s\Delta\omega L_f i_{d0} + s\omega_0 L_f \Delta i_d) + \Delta i_q (s\omega_0 L_f \Delta i_q + s\Delta\omega L_f i_{q0}) dt \\ &+ \int (\Delta i_d s\Delta e_{gq} - \Delta i_q s\Delta e_{gd}) dt + \int \Delta i_d \Delta i_q (sk_{pd} + k_{id}) dt \\ &= \Delta V_{I1} + \Delta V_{I2} + \Delta V_{I3} + \Delta V_{I4} \end{aligned} \tag{14}$$

In the equation, ΔV_{I1} is mainly affected by the k_{pq} and k_{iq}; ΔV_{I2} is the energy dominated by the dq-axis cross-coupling term; ΔV_{I3} is the energy dominated by the dq-axis voltage feedforward term; and ΔV_{I4} is mainly affected by the k_{pd} and k_{id}.

The energy expression dominated by phase-locked control is as follows:

$$\begin{aligned} \Delta V_{PLL} &= \int C_{dc} U_{dc0} \Delta U_{dc} \Delta i_q (k_{ip} + k_{pp}s)(k_{pq} + k_{iq}\tfrac{1}{s}) dt \\ &- \int C_{dc} U_{dc0} \Delta U_{dc} (k_{ip} + k_{pp}s)(\Delta\omega L_f i_{d0} + \omega_0 L_f \Delta i_d) dt \\ &- \int C_{dc} U_{dc0} \Delta U_{dc} \Delta e_{gq} (k_{ip} + k_{pp}s) dt \\ &= \Delta V_{PLL1} + \Delta V_{PLL2} + \Delta V_{PLL3} \end{aligned} \tag{15}$$

According to the derived expression, it can be seen that ΔV_{PLL1} is mainly affected by the control parameters of the phase-locked loop and the parameters of the q-axis current loop; ΔV_{PLL2} is the energy dominated by the interaction between the phase-locked loop and the dq-axis cross-coupling term. ΔV_{PLL3} is mainly affected by the q-axis voltage feedforward term and the control parameters of the phase-locked loop.

3. Sensitivity Analysis

The conventional approach to sensitivity analysis primarily involves using analytical techniques. For the refined energy function of D-PMSG, the sensitivity expression is the following:

$$S_i = \frac{\partial \Delta V}{\partial \Delta x} \tag{16}$$

where S_i is the sensitivity of the i-th variable and x-related variables.

While Equation (16) is capable of computing sensitivity, bringing refined energy function into this method involves a more complex procedure. As a result, the perturbation strategy is used in this study to ascertain each variable's sensitivity inside the refined energy function.

By measuring the energy levels immediately prior to and following the disturbance after deploying the identical disturbance to all state variables, it is possible to ascertain the impact of state variables on energy. Equation (17) displays the energy levels both before and after the disturbance:

$$\begin{cases} V_{p1} = f(x) \\ V_{p2} = f(x + \Delta x) \end{cases} \tag{17}$$

Among them are V_{p1}—V before applying disturbance; V_{p2}—V after applying disturbance; the correlation between f-state variables and energy in terms of their functions; x-state variable; and Δx—perturbation.

The impact of each variable is quantified using Equation (18). By deducting the pre-disturbance energy from the post-disturbance energy for each data point and taking the average's absolute value, the required measure is derived. The notation for this measurement is S_V, and it is known as the sensitivity of the state variable to energy.

$$S_V = \overline{|V_{p1} - V_{p2}|} \tag{18}$$

Since each state variable applies the same disturbance, only the difference in energy can be compared to see the state variable's impact on the energy. Furthermore, as the disturbance occurs simultaneously, it is possible to negate the effect of the initial steady state. This enables the determination and ranking of sensitivity values S_V for each state variable. The variable with the highest S_V shows the greatest energy sensitivity. Thus, identifying one or more such highly sensitive state variables is feasible. Adjusting these key state variables allows for the effective modulation of D-PMSG's refined energy function, facilitating energy control.

The D-PMSG state variables are divided into five parts, and the specific state variables related to each part of the D-PMSG are shown in Table 2.

Table 2. State variable grouping.

Module	Corresponding State Variables
Shafting	Fan speed ω_s
Direct-drive permanent magnet synchronous generator	Stator d, q axis current i_{ds}, i_{qs}
Converter	Direct current voltage u_{dc} Fixed d-axis current of machine-side converter x_1 The fixed speed of the outer ring and inner ring of the machine-side converter x_2, x_3 The outer ring and inner ring of the grid-side converter are fixed DC voltage x_4, x_5 Fixed q-axis current of grid-side converter x_6
Collecting power lines	The d-axis and q-axis currents at the outlet of the grid-side converter i_{dg}, i_{qg} The d-axis and q-axis voltage of the grid-side converter outlet u_{dg}, u_{qg}
PLL	x_a, x_b

The associated variables are the d and q axis components d and q, and the state variables of the PLL are represented by x_a and x_b in Table 2. The following expressions include the values for variables x_1 through x_6, where the variable reference has a given value.

$$\begin{cases} \frac{dx_a}{dt} = u_{qg} \\ \frac{dx_b}{dt} = \omega_0 + u_{qg}k_{ppll} + u_{qg}T_{ipll} = \omega \end{cases} \tag{19}$$

$$\begin{cases} \frac{dx_1}{dt} = i_{dsref} - i_{ds} \\ \frac{dx_2}{dt} = \omega_{sref} - \omega_s \\ \frac{dx_3}{dt} = i_{qsref} - i_{qs} \\ \frac{dx_4}{dt} = u_{dc} - u_{dcref} \\ \frac{dx_5}{dt} = i_{dgref} - i_{dg} \\ \frac{dx_6}{dt} = i_{qgref} - i_{qg} \end{cases} \tag{20}$$

4. Results Simulation Analysis

This section firstly builds the corresponding electromagnetic transient model in MATLAB/SIMULINK 2020b, calculates the port transient energy of D-PMDG based on the measured electrical quantities, and compares it with the total of the improved energy function that is suggested in this study. Then, it is demonstrated that the approach suggested in this research may be used in the field of SSO-disturbance-source location in the two scenarios of forced-oscillation-type SSO and weak damping-type SSO. Moreover, the method flow chart used in this study is shown in Figure 2.

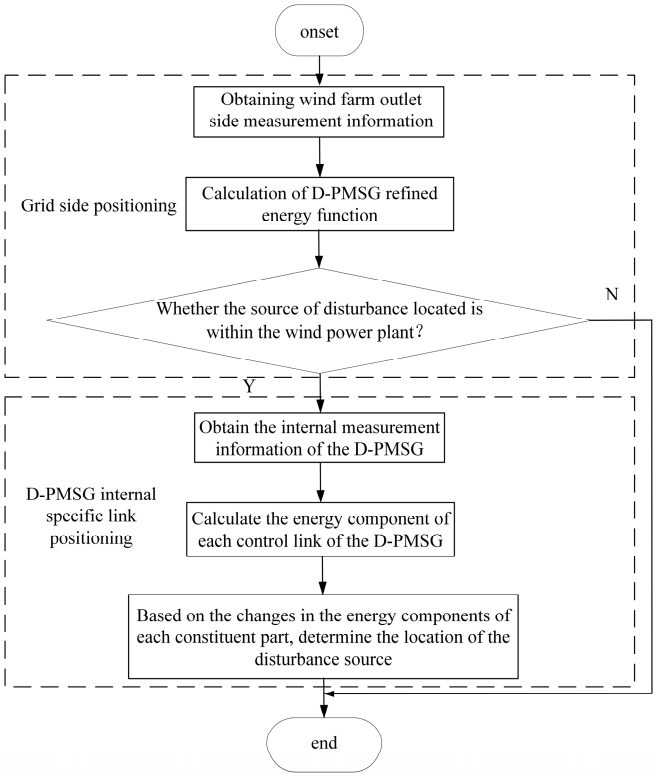


Figure 2. The process diagram of the method used in this paper.

4.1. Validation of the Technique

With the purpose of authenticating the correctness of the proposed technique, the decomposed energy is compared with the exterior features of the D-PMSG. The external characteristic mentioned here is to regard the output of D-PMSG as the load power with negative power. By figuring out the load energy, the calculation equation of load energy

is introduced to replace the energy of D-PMSG, which is called the external characteristic energy later. This investigation verifies the applicability of the energy function model to the later SSO analysis if the external characteristic energy agrees with the refined energy that was established in this paper. And on the basis of this analysis, the remaining properties of the energy function generated are examined.

For the purpose of facilitating the investigation of the generated energy function's characteristics, D-PMSG is linked to the infinite bus system. At 3 s into the simulation and extending to the conclusion, the D-PMSG has a connection to the weak AC grid. The external-characteristic energy curve of D-PMSG and the constructed refined-energy curve are shown in Figure 3. The difference can be made between the external-characteristic calculation and the refined-energy-function curve generated by this study since both of them are a simplified D-PMSG energy and the second is not the actual energy of D-PMSG. Additionally, there is some inconsistency in the curves generated through the two energy functions as a result of issues like measurement errors and model discrepancies. This paper's energy function is going to go through several integrations, and initially not many deviations will progressively increase. Therefore, this paper only makes a qualitative comparison, and the elimination of errors will be studied in detail in the future. It can be demonstrated from the figure that the refined-energy-function curve's trend and the energy curve derived from the external characteristic data are essentially consistent. As a result, to some extent, the energy function established during the present investigation may symbolize the energy of D-PMSG.

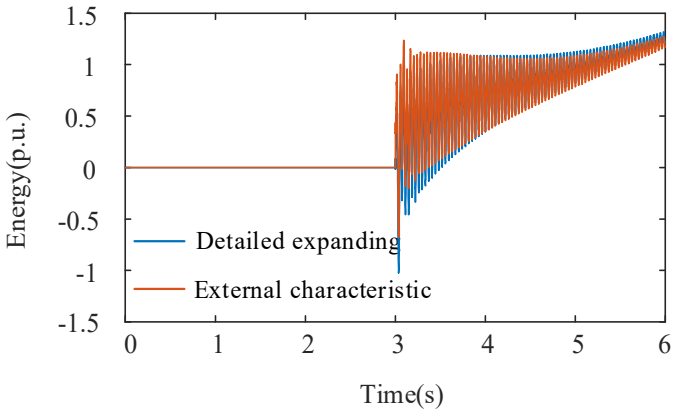


Figure 3. Comparison of energy curves between amplitude-phase motion-equation model and simulation model.

4.2. Example Analysis

(1) Weak damping-type SSO

Weak damping oscillation may occur in the power grid under certain conditions, such as power grid failure, load mutation, the failure of control measures, etc. If effective measures are not taken in time to suppress it, it could represent a risk to the stable and secure functioning of the electrical grid. Therefore, this paper focuses on the SSOs of the weak damping type.

Using the simulation system depicted in Figure 1 as a foundation, the D-PMSG is switched from an infinite system to a weak AC system in the third second after the simulation starts; that is, the relative strength of the D-PMSG connected to the system is weakened and continues until the simulation concludes. Currently, Figure 4 displays the active power output of the D-PMSG. The weak damping-type attenuation oscillation of the system is evident.

The Lyapunov second stability principle states that if the free dynamical system's total energy V changes at a constant negative rate with respect to time ΔV, The overall energy of the system will continue to decrease, maintaining system stability. On the contrary, when

ΔV is constantly positive, the system stability will gradually decline as the system's overall energy continues to rise. Therefore, the buildup and consumption pattern of total energy can be used to assess the stability of D-PMSG.

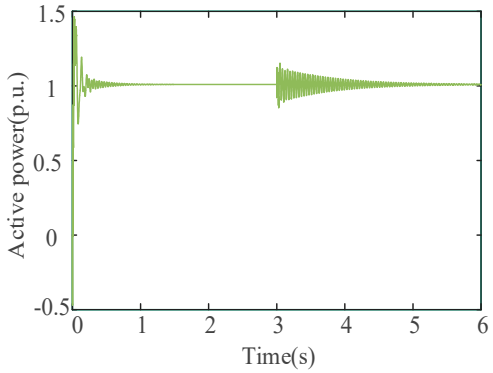


Figure 4. D-PMSG output active-power curve (weak damping-type SSO).

The energy-function equation is dominated by each control link in the grid-side converter, as deduced in the Section 2. The specific distribution of the internal energy of D-PMSG is obtained as shown in Figure 5. From the diagram, it can be seen that the energy component dominated by the phase-locked loop is larger. Of these energy constituents, ΔV_{PLL1} tied to the PI parameters of the phase-locked loop and the q-axis current loop is much larger than other energy components, and its energy-change rate is positive, leading to the system's continual negative damping properties and transient energy. Furthermore, unstable SSO may occur in the system. The energy dominated by the DC voltage control link and the energy dominated by the D-axis current loop account for a relatively small proportion of the system, and the energy-change rate is negative. An increase in these two energy components will strengthen the system's favorable damping effect in the sub-synchronous frequency range and increase its degree of stability. We infer that the SSO issue this scenario exhibits is the result of an interaction between the phase-locked loop and the q-axis current loop (Figure 5).

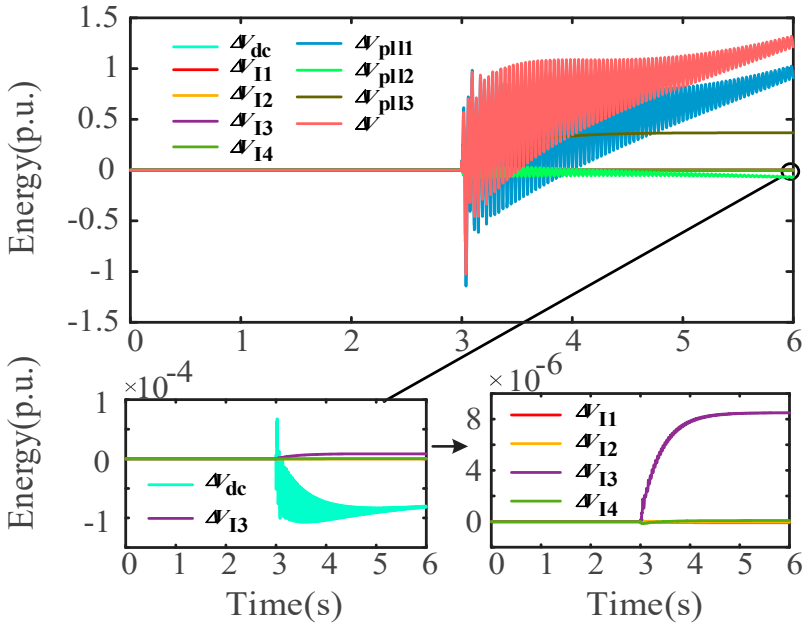


Figure 5. D-PMSG refine energy curve.

According to the improved perturbation method and the state variable grouping proposed in the Section 3, the system is analyzed. The sensitivity analysis results show that the state variables x_a, x_b, corresponding to the D-PMSG phase-locked loop control and the q-axis component i_{gq} of the D-PMSG grid-side current flowing to the AC network as shown in Figure 6, are mainly involved in the SSO phenomenon, which is consistent with the results based on the refined energy analysis.

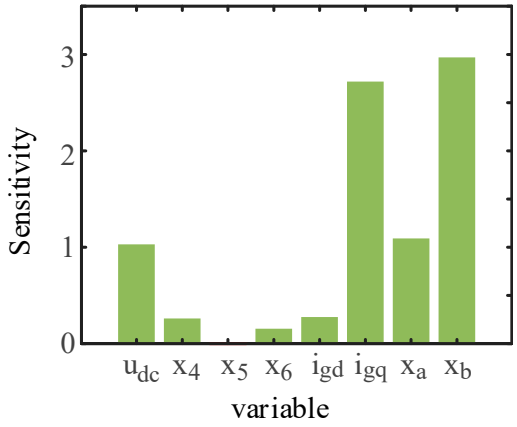


Figure 6. Sensitivity of each state variable.

(2) Forced-oscillation-Type SSO

In the mechanism depicted in Figure 1, a sinusoidal current source is added to the high-voltage side of the transformer T2 at the outlet of the D-PMSG. There is a 25 Hz oscillation with an amplitude of 2 kA. The disturbance starts at the third second of the simulation and continues until the end. The output port's active-power curve can be shown in Figure 7, and it is clear that the system oscillates with exactly the same amplitude.

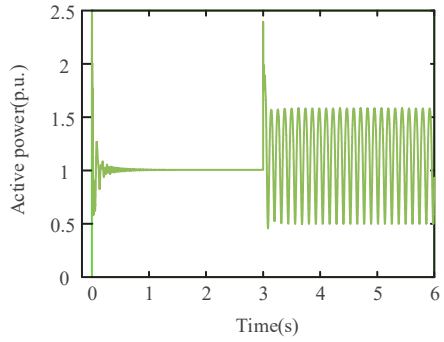


Figure 7. D-PMSG output active-power curve (forced-oscillation-type SSO).

The energy components that each grid-side converter control link dominated and the total energy synthesized are shown in Figure 8. It can be seen that the energy-change rate is dominated by the DC voltage control, and the energy-change rate is dominated by the dq-axis cross-coupling term, while the phase-locked loop and the q-axis current loop combine to dominate the energy-change rate, which is positive. It can be indicated that these components provide the system with negative damping energy. In line with the disturbance-source-setting result, the total energy-change rate of D-PMSG is negative, demonstrating that the disturbance source is not inside the wind turbine.

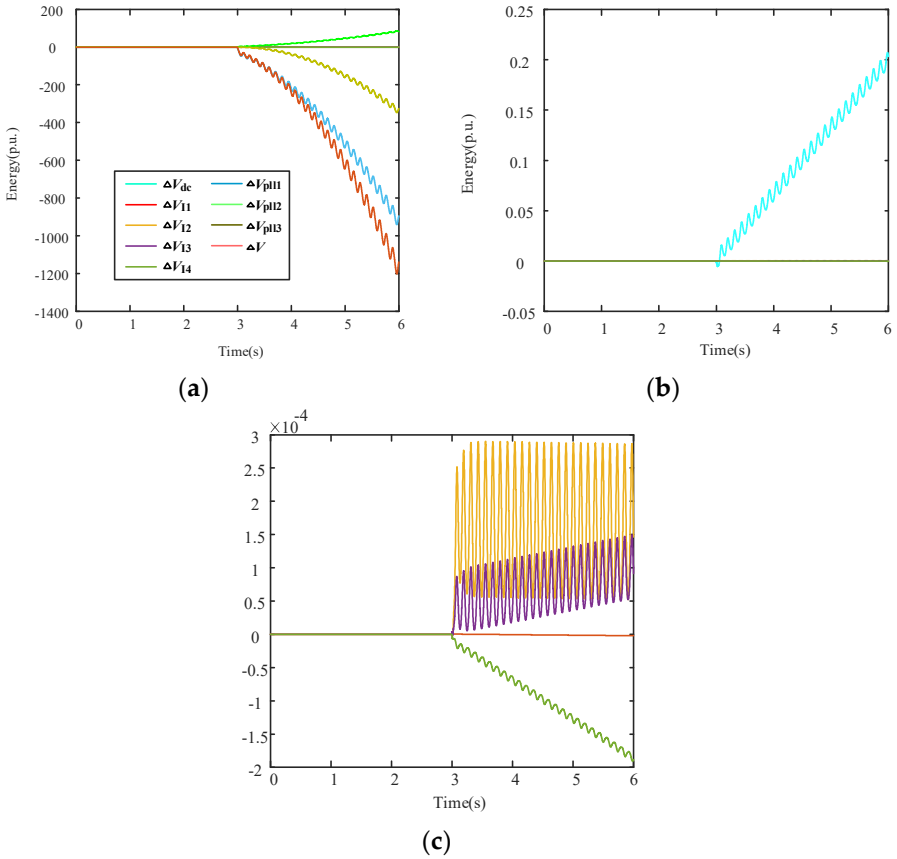


Figure 8. Refined energy decomposition diagram: (**a**) synthesize the total energy and the energy component dominated by the phase-locked loop; (**b**) the DC voltage ring dominated the energy component; and (**c**) the energy component dominated by the current loop.

5. Conclusions

The primary goal of the current research on sub-synchronous oscillation-disturbance-source localization for grid-connected D-PMSG is to determine if the disturbance source is situated on the generator side or the grid side of the D-PMSG, or if it is internal to the D-PMSG. On the other hand, the internal components' particular control loop has not been thoroughly examined. This study explores the construction of a refined energy function for D-PMSG from an energy perspective. This will allow for the localization of disturbance sources within certain D-PMSG control loops during sub-synchronous oscillation (SSO). The analysis results are verified by analyzing the sensitivity of different parameters to energy. The following are this paper's primary contributions:

(1) The development of an improved D-PMSG energy function. A layered analysis is performed based on the small-signal models of different control loops in D-PMSG, and transient energy methods are used to meticulously analyze the energy structure. As a result, a refined-energy function that captures the dynamic properties of D-PMSG and accounts for its internal control loops is developed. In the example study employed in this research, it is observed through simulations in SIMULINK that the majority of the energy of D-PMSG is concentrated in the phase-locked loop;

(2) The identification of internal state variables in D-PMSG that exhibit high sensitivity to energy. By improving upon the traditional perturbation method, a sensitivity analysis is conducted on various state variables of D-PMSG with respect to the refined-energy function constructed in this paper. The analysis reveals that, in the case study used here, the state variables x_a, x_b, corresponding to the D-PMSG phase-locked loop control and the q-axis component i_{gq} related to phase-locked loop control, are

primarily involved in SSO phenomena, which aligns with the results obtained through the disturbance-source-localization method employed in this paper;

(3) The validation of the suggested approach within the framework of forced-oscillation SSO. A forced-oscillation SSO scenario is created in SIMULINK simulations by putting the disturbance source on the grid side. The efficacy of the suggested approach is validated when the disturbance source is found not to originate from within D-PMSG using the disturbance-source-localization method employed in this work.

Using the improved energy function this study produced, the future construction of additional damping controllers for important control loops that affect the incidence of SSO is the goal of this paper. This method provides a fresh viewpoint on the coordinated control of networked power grids that use D-PMSG, which improves stability and dependability in power systems that rely on renewable energy.

Author Contributions: Conceptualization, methodology, investigation, resources, writing—review and editing, visualization, C.L. and Z.Z.; software, formal analysis, writing—original draft, data curation, S.Z., S.G., J.Y. and Z.C. All authors have read and agreed to the published version of the manuscript.

Funding: The authors declare that this study received funding from the JBGS project 'Research and Application of Key Technologies for Identification and Early Warning of Broadband Oscillation in Jilin Power Grid' which is supported by State Grid Jilin Electric Power Co., Ltd. The funder had the following involvement with the study: the collection, analysis, or interpretation of data.

Data Availability Statement: The data presented in this study are available on request from the corresponding author. The data are not publicly available due to that the project involved in the manuscript is not yet completed and is not in the public stage.

Conflicts of Interest: Author Jingying Yang was employed by State Grid Jilin Electric Power Company Limited. Authors Shuyu Zhou and Song Gao were employed by the company State Grid Jilin Electric Power Research Institute. The remaining authors declare that the research was conducted in the absence of any commercial or financial relationships that could be construed as a potential conflict of interest.

References

1. Yang, D.; Sun, Y. Generalized Impedance-Based Stability Analysis for System- Level Small-Signal Stability Assessment of Large-Scale Power Electronics-Dominated Power Systems. In Proceedings of the 2021 IEEE 12th Energy Conversion Congress & Exposition—Asia (ECCE-Asia), Virtual, 24 May 2021; IEEE: Singapore; pp. 2069–2074.
2. Xiao, X.; Luo, C.; Liao, K. Review of the Research on Subsynchronous Oscillation Issues in Electric Power System with Renewable Energy Sources. *Diangong Jishu Xuebao/Trans. China Electrotech. Soc.* **2017**, *32*, 85–97.
3. Xie, X.; Zhang, X.; Liu, H.; Liu, H.; Li, Y.; Zhang, C. Characteristic Analysis of Subsynchronous Resonance in Practical Wind Farms Connected to Series-Compensated Transmissions. *IEEE Trans. Energy Convers.* **2017**, *32*, 1117–1126. [CrossRef]
4. Shao, B.; Zhao, Z.; Xiao, Q.; Yang, Z.; Meng, X. Weak Robustness Analysis of Close Subsynchronous Oscillation Modes' Participation Factors in Multiple Direct-Drive Wind Turbines with the VSC-HVDC System. *Diangong Jishu Xuebao/Trans. China Electrotech. Soc.* **2023**, *38*, 754–769.
5. Adams, J.; Carter, C.; Huang, S.-H. ERCOT Experience with Sub-Synchronous Control Interaction and Proposed Remediation. In Proceedings of the PES T&D 2012, Orlando, FL, USA, 7–10 May 2012; IEEE: Orlando, FL, USA; pp. 1–5.
6. Sun, Z.; Cai, G.; Yang, D.; Liu, C.; Wang, B.; Wang, L. A Method for the Evaluation of Generator Damping During Low-Frequency Oscillations. *IEEE Trans. Power Syst.* **2019**, *34*, 109–119. [CrossRef]
7. Ma, J.; Wang, L.; Shen, Y. Interaction Energy-Based Stability Analysis Method and Application in Grid-Tied Type-4 Wind Turbine Generator. *IEEE J. Emerg. Sel. Top. Power Electron.* **2021**, *9*, 5542–5557. [CrossRef]
8. Chen, X.; Wu, X.; Gu, W.; Fan, L. Research on Energy Analysis and SSO Source Location Method for Power Grids with DFIGs Based on the Sub-Synchronous Modal Energy. *Zhongguo Dianji Gongcheng Xuebao/Proc. Chin. Soc. Electr. Eng.* **2023**, *43*, 5863–5876.
9. Chen, W.; Yu, X.; Han, X.; Jia, Y.; Chang, X.; Guo, X. Analysis of Forced SSOs Excited by Subsynchronous Interharmonics From DPMSG-Based Wind Farms. *IEEE Trans. Sustain. Energy* **2021**, *12*, 978–989. [CrossRef]
10. Xie, X.; Zhan, Y.; Shair, J.; Ka, Z.; Chang, X. Identifying the Source of Subsynchronous Control Interaction via Wide-Area Monitoring of Sub/Super-Synchronous Power Flows. *IEEE Trans. Power Deliv.* **2020**, *35*, 2177–2185. [CrossRef]
11. Gao, B.; Wang, Y.; Xu, W.; Yang, G. Identifying and Ranking Sources of SSR Based on the Concept of Subsynchronous Power. *IEEE Trans. Power Deliv.* **2020**, *35*, 258–268. [CrossRef]

12. Chen, L.; Min, Y.; Hu, W. Low Frequency Oscillation Analysis and Oscillation Source Location Based on Oscillation Energy. Part One: Mathematical Foundation and Energy Flow Computation. *Dianli Xitong Zidonghua/Autom. Electr. Power Syst.* **2012**, *36*, 22–27+86.
13. Maslennikov, S.; Wang, B.; Litvinov, E. Dissipating Energy Flow Method for Locating the Source of Sustained Oscillations. *Int. J. Electr. Power Energy Syst.* **2017**, *88*, 55–62. [CrossRef]
14. Maslennikov, S.; Litvinov, E. ISO New England Experience in Locating the Source of Oscillations Online. *IEEE Trans. Power Syst.* **2021**, *36*, 495–503. [CrossRef]
15. Liu, C.; Diao, S.; Cai, G.; Zhang, Y.; Yu, F. Construction of Detailed Energy Function of Double-fed Induction Generator for Small Signal Stability Analysis of Power Systems with a High Penetration of Double-fed Induction Generator. *IET Gener. Trans. Dist.* **2022**, *16*, 4761–4774. [CrossRef]
16. Wu, M.; Xie, L.; Cheng, L.; Sun, R. A Study on The Impact of Wind Farm Spatial Distribution on Power System Sub-Synchronous Oscillations. *IEEE Trans. Power Syst.* **2016**, *31*, 2154–2162. [CrossRef]
17. Perera, U.; Oo, A.M.T.; Zamora, R. Sub Synchronous Oscillations under High Penetration of Renewables—A Review of Existing Monitoring and Damping Methods, Challenges, and Research Prospects. *Energies* **2022**, *15*, 8477. [CrossRef]
18. Yan, X.; Chang, W.; Cui, S.; Rasool, A.; Jia, J.; Sun, Y. Recurrence of Sub-Synchronous Oscillation Accident of Hornsea Wind Farm in UK and Its Suppression Strategy. *Energies* **2021**, *14*, 7685. [CrossRef]
19. Mourabit, Y.E.; Salime, H.; Bossoufi, B.; Motahhir, S.; Derouich, A.; Mobayen, S.; Zhilenkov, A. Enhanced Performance in PMSG-Based Wind Turbine Systems: Experimental Validation of Adaptive Backstepping Control Design. *Energies* **2023**, *16*, 7481. [CrossRef]
20. Ashraf, A.; Saadi, M. The Impact of Phase-Locked Loop (PLL) Architecture on Sub-Synchronous Control Interactions (SSCI) for Direct-Driven Permanent Magnet Synchronous Generator (PMSG)-Based Type 4 Wind Farms. *World Electr. Veh. J.* **2023**, *14*, 206. [CrossRef]
21. Chao, W.; Deng, C.; Huang, J.; Dai, L.; Min, Y.; Cheng, Y.; Wang, Y.; Liao, J. A Sub-Synchronous Oscillation Suppression Strategy Based on Active Disturbance Rejection Control for Renewable Energy Integration System via MMC-HVDC. *Electronics* **2023**, *12*, 2885. [CrossRef]

Disclaimer/Publisher's Note: The statements, opinions and data contained in all publications are solely those of the individual author(s) and contributor(s) and not of MDPI and/or the editor(s). MDPI and/or the editor(s) disclaim responsibility for any injury to people or property resulting from any ideas, methods, instructions or products referred to in the content.